WEATHER CLIMATE WATER

WORLD METEOROLOGICAL ORGANIZATION

GLOBAL SEASONAL CLIMATE UPDATE

TARGET SEASON: September-October-November 2026

Prepared: 20 August 2026

Summary

(Prepared – 20 August 2026)

Observed Oceanic Drivers for the Previous Season: During the May–July 2026 (MJJ 2026) season, warm sea surface temperature (SST) anomalies dominated global oceans. A rapid intensification of above-normal SST anomalies occurred across the central and eastern equatorial tropical Pacific. From May 2026 to July 2026, the monthly Niño 3.4 index surged from 0.9°C to 2.0°C. For the season as a whole, all Niño indices were firmly in above-normal territory, reflecting well-established El Niño conditions across the equatorial Pacific.

In other ocean basins, the Indian Ocean Dipole (IOD) hovered in negative territory, driven by stronger *relative* warming in the eastern equatorial Indian Ocean compared to the west. Meanwhile, positive SST anomalies persisted across the equatorial and subtropical Atlantic, with SST anomalies in the North Tropical Atlantic (NTA) and South Tropical Atlantic (STA) remaining slightly above average. Concurrently, widespread positive SST anomalies continued to dominate the North Pacific[1].

Outlook for Oceanic Drivers for the Next Season: For the September–November 2026 (SON 2026) season, multi-model ensemble (MME) forecasts indicate a further development toward stronger El Niño conditions. The seasonal average Niño 3.4 SST ensemble mean anomaly is forecast to reach approximately 3.6°C during SON 2026, with the intensification trajectory peaking in November-December. The spread among individual forecast systems generally remains narrow, reflecting high forecast confidence.

In the Indian Ocean, a positive IOD phase is also expected to develop, reaching an SON 2026 seasonal mean value of 0.9°C. Meanwhile, the equatorial Atlantic basin is forecast to remain generally warm, with SSTs in both the North and South Tropical Atlantic staying above normal.

Surface Temperature Outlook for the Next Season: For the SON 2026 season, multi-model ensemble forecasts project a nearly universal global dominance for enhancement in **probabilities** for above-normal temperatures over landmasses. This warming trend is especially pronounced north of 60°S, where a large increase in probabilities for above-normal temperature is reinforced by high model consistency.

In the Northern Hemisphere, a large increase in probabilities for above-normal temperatures covers Africa, southern Europe, the Arabian Peninsula, the Indian Subcontinent, eastern Asia, western coastal parts of North America below 60°N, northeastern regions of North America, Central America, the Caribbean, and the Arctic Circle above 60°N. Model consistency across these regions is moderate to strong. Conversely, a weaker enhancement in probabilities of above-normal temperatures is indicated over parts of northern Asia, as well as northwestern and central regions of North America.

In the Southern Hemisphere, a strong enhancement in probabilities for above-normal temperatures is centred over southern Africa, South America between the equator and 30°S, most of Australia, and across New Zealand, supported by strong model consistency.

In the tropics, a large increase in probabilities for above-normal temperatures covers equatorial Africa, South America, and western parts of the Maritime Continent. Over the ocean basins, forecasts reflect the footprint of a strong El Niño event. Extreme probabilities (exceeding 80%) for above-normal SSTs dominate the equatorial Pacific east of the Date Line, where the core of the warm region displays maximum model consistency.

A widespread tendency for an increase in probabilities for above-normal temperatures also covers the Indian Ocean and the tropical Atlantic. In contrast, a region of enhancement for below- to near-normal temperature probabilities is predicted across the subpolar North Atlantic. Additionally, a

[1] https://www.cpc.ncep.noaa.gov/products/attribution/images/Attribution202607.pdf

distinct zone of enhanced probabilities for below-normal temperatures is centred in the South Pacific subtropical region (between 10°S and 30°S) situated directly south of the core El Niño region, supported by strong model consistency.

Rainfall Outlook for the Next Season: For the SON 2026 season, MME forecasts display well-structured, large tilts in rainfall **probabilities**, exhibiting a classic, strong atmospheric response to Pacific El Niño. The most dominant feature of the SON 2026 outlook is a strong enhancement in the probability of above-normal rainfall stretching across the central and eastern equatorial Pacific east of the Date Line, backed by strong model consistency. The core for this rainfall signal is flanked by an extensive region of below-normal rainfall probabilities to the east and the west. This broad dry signal encompasses widespread marine zones, manifesting as strong enhancements in the probability for below-normal rainfall over both the tropical Indian Ocean and the equatorial Atlantic Ocean, as well as a horseshoe pattern extending into the Northern and Southern Hemispheres starting at around 120°E. The southern lobe of enhancement in below-normal probability stretches across the South Pacific to the southern tip of South America.

The Indian Subcontinent features an enhancement in the probability for below-normal rainfall, exhibiting high model consistency across the region. To its northwest, there is an enhancement in probabilities for above-normal rainfall extending into parts of Central Asia and northern regions of the Arabian Peninsula. Across equatorial Africa, the Greater Horn of Africa shows an enhanced probability for above-normal rainfall, with an enhancement in probability for below-normal rainfall to its west. Flanking this equatorial belt, a weak enhancement in the probability for above-normal rainfall is indicated over northern Africa.

Over North America, there is an enhancement in the probability for below-normal rainfall covering the southern parts of Central America and the Caribbean, supported by high model consistency. To its north, there is an enhancement in the probability of above-normal rainfall over parts of North America south of 45°N. In South America, a robust enhancement in probability for below-normal rainfall is centered over the northwest, continuing steadily along the northern coastal areas to the east. Farther south, a branch of enhanced probability for above-normal rainfall extends across southeastern South America, giving way to an enhanced probability for below-normal rainfall over the southern tip of the continent.

Across Europe, the forecasts reveal a notable latitudinal split. An enhancement in the probability of above-normal rainfall covers the southern parts of Europe, whereas the predicted signal is weak across northern Europe. The consistency is low to moderate.

Over Australia, the predicted signal is weak.

How to use the Global Seasonal Climate Update: Figure 1 displays the seasonal outlook maps, which illustrate the **probabilities** of seasonal mean surface temperature (left) and precipitation (right) falling into above-, near-, or below-normal categories relative to local climatology. The color coding identifies the category with the **highest forecast probability**. For example, red, blue, or grey regions indicate that the seasonal mean surface air temperature is most likely to be above-, below-, or near-normal, respectively. **Deeper shades** reflect a higher probability of the seasonal mean falling into that dominant category, while **white areas** denote equal chances (33.3% each) for all three categories. Crucially, colors indicate **probability rather than certainty**; there remains a **non-zero chance** that the observed seasonal mean may fall into a category other than the one mapped as most likely.

Probability Forecast for Surface Air Temperature SON 2026 | **Probability Forecast for Precipitation SON 2026**

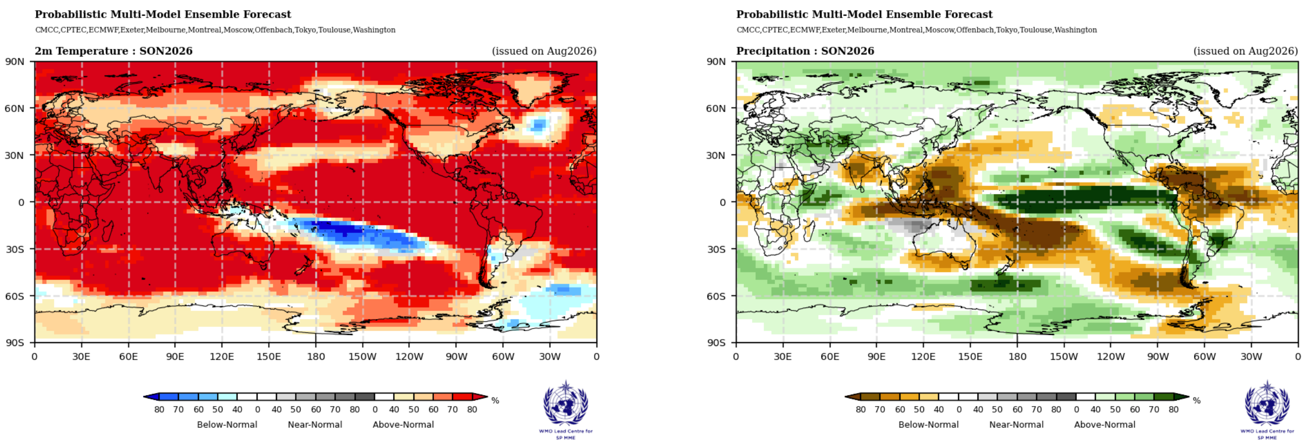

Figure 1. Probabilistic forecasts of surface air temperature and rainfall for the season September-November 2026. The tercile category with the highest forecast probability is indicated by shaded areas. The most likely category for below-normal, above-normal, and near-normal is depicted in blue, red, and grey shadings respectively for temperature, and yellow, green and grey shadings respectively for rainfall. White areas indicate equal chances for all categories in both cases. The baseline period is 1993–2009. (*Source:* The WMO Lead Centre for Seasonal Prediction Multi-Model Ensemble)

1. Observations: May-July 2026

In the following sections, observed temperature and rainfall patterns for the previous season are discussed. For more detailed information about regional and local climate anomalies, the reader is referred to the concerned WMO Regional Climate Centres (RCCs) or RCC Networks, listed in Section 5.

1.1 Large-scale sea-surface temperature (SST) indices

During the May–July 2026 (MJJ 2026) season, warm sea surface temperature (SST) anomalies dominated global oceans. A rapid intensification of above-normal SST anomalies occurred across the central and eastern equatorial tropical Pacific. From May 2026 to July 2026, the monthly Niño 3.4 index surged from 0.9°C to 2.0°C. For the season as a whole, all Niño indices were firmly in above-normal territory, reflecting well-established El Niño conditions across the equatorial Pacific.

In other ocean basins, the Indian Ocean Dipole (IOD) hovered in negative territory, driven by stronger relative *warming* in the eastern equatorial Indian Ocean compared to the west. Meanwhile, positive SST anomalies persisted across the equatorial and subtropical Atlantic, with SST anomalies in the North Tropical Atlantic (NTA) and South Tropical Atlantic (STA) remaining slightly above average. Concurrently, widespread positive SST anomalies continued to dominate the North Pacific.

Month	Niño 1+2	Niño 3	Niño 4	Niño 3.4	IOD	NTA	STA
May 2026	1.8	1.1	1.0	0.9	-0.4	0.2	0.3
June 2026	2.8	1.8	1.2	1.6	-0.6	0.2	0.3
July 2026	3.6	2.3	1.1	2.0	-0.1	0.4	0.2
May-July 2026	2.7	1.7	1.1	1.5	-0.4	0.3	0.3

Table 1. Large-scale oceanic indices (°C). Anomalies are with respect to the 1991–2020 average. (*Source:* U.S. Climate Prediction Center)

1.2 Observed land temperature

During the MJJ 2026 season, near-global warmth dominated land surface temperatures, with widespread positive anomalies observed across most continents (Figure 2, top). Regions with the largest warming were located over equatorial eastern Africa, western Europe, northern parts of Asia, and the far northeastern region of North America. Warming was also observed over the western lower half of North America, Central America, the Caribbean, most of South America north of 25°S, western and southern Africa below the equator, eastern Australia, and New Zealand. While scattered patches of below-normal temperatures were observed over the Arabian Peninsula, parts of eastern Asia, and northwestern parts of Australia, the only region with systematic cold anomalies was northwestern North America.

Over the oceans, above-normal temperatures also dominated. The warmest temperature anomalies were located in the equatorial Pacific associated with El Niño conditions, along the western coasts of Central America and South America (north of 30°S), and along 45°N in the extratropical Pacific Ocean extending into the coastal regions of Eastern Asia.

Over land areas, regions with warm extremes (exceeding all seasonal mean temperatures observed during 1991–2020) included western Europe, equatorial eastern parts of Africa, coastal regions of eastern Asia, far northeastern parts of North America, and the Caribbean (Figure 2, bottom). Over the oceans, warm extremes were observed near the Date Line, extending northeastward towards Central America into the Caribbean, along 45°N in the extratropical Pacific, and across scattered regions in the southern Pacific, the Atlantic, and the Indian Ocean. No regions with cold extremes were observed.

1.3 Observed land rainfall

During the MJJ 2026 season, observed rainfall anomalies reflected a distinct tropical response consistent with El Niño conditions, alongside notable extratropical regional contrasts (Figure 3, top).

Across land areas, suppression in seasonal mean rainfall dominated over the central region of North America, southern Greenland, southern parts of Central America, the Caribbean, northern South America, equatorial eastern Africa, the Maritime Continent, and western and southern Europe. In contrast, above-normal rainfall was observed across parts of southern and northern North America, regions of East Asia, parts of Central Asia, equatorial West Africa bordering the northern Gulf of Guinea, western parts of southern South America, and western coastal regions of equatorial South America.

Over the ocean basins, a strong positive rainfall anomaly band stretched across the central and eastern equatorial Pacific east of the Date Line, flanked by dry anomalies to the north and south. Broad regions of below-normal rainfall anomalies dominated the tropical Indian Ocean, the Maritime Continent, the western tropical Pacific, and the equatorial Atlantic.

In percentile terms, dry extremes (below all seasonal mean rainfall observed during 1991–2020) were recorded across western Europe, parts of the western Caribbean, far northeastern parts of North

America, regions near the Horn of Africa, and portions of the eastern Maritime Continent (Figure 3. bottom). Patches of wet extremes were scattered over equatorial Africa, and Southeast Asia.

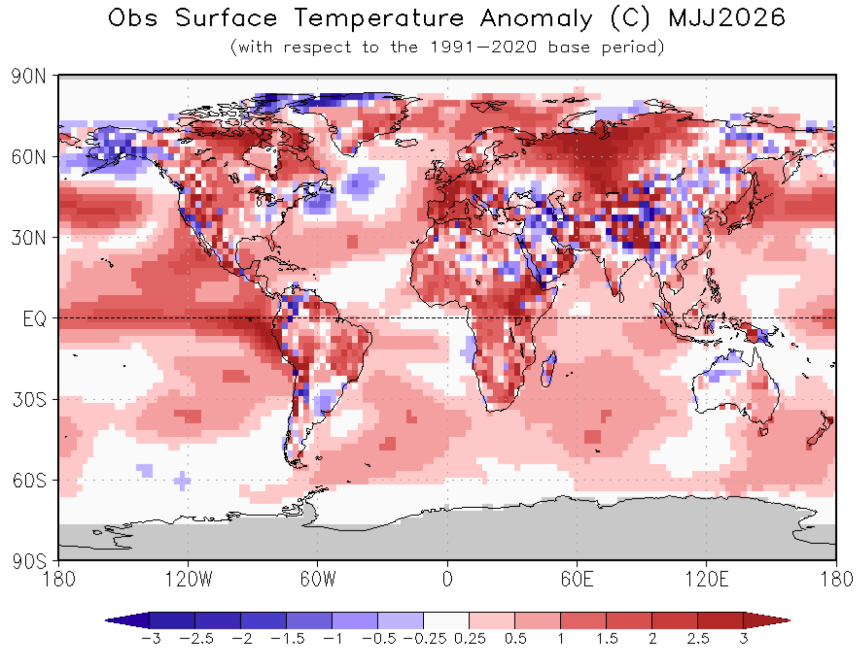

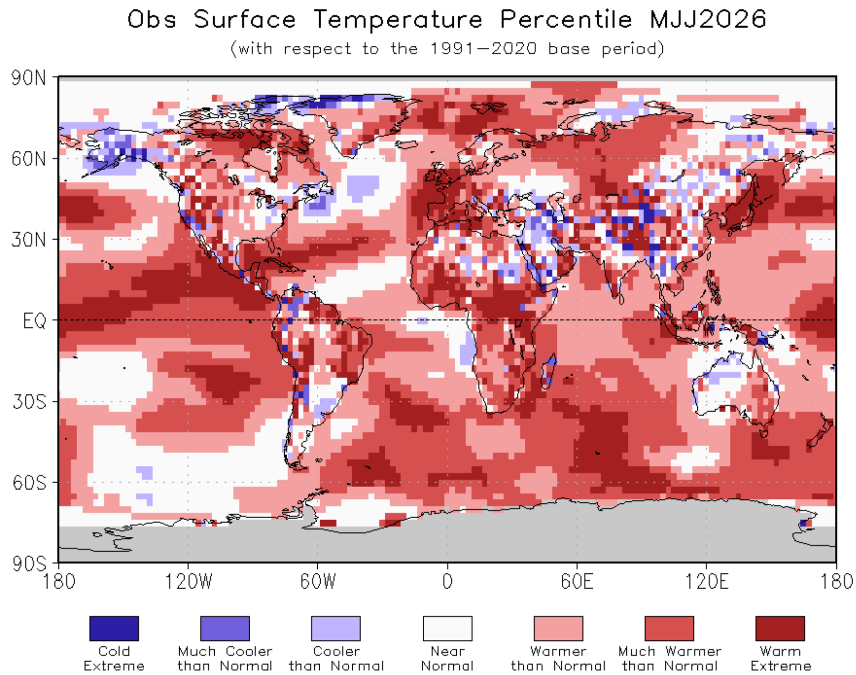

Figure 2. Observed May-July 2026 near-surface temperature anomalies (ºC) relative to 1991–2020 (top). The *Cooler than Normal, Near Normal, and Warmer than Normal* shadings on the percentile map (bottom) indicate that seasonal

mean anomalies were in the bottom, middle, and upper tercile of the 1991–2020 distribution, respectively. Regions with anomalies in the lowest and highest decile (or 10%) of the distribution are marked as *Much Cooler than Normal* and *Much Warmer than Normal*, respectively. The *Cold Extreme* and *Warm Extreme* shadings indicate that the anomalies exceeded the coldest and warmest temperature values of the 1991–2020 period for the season. Grey shading indicates areas where observational analysis was not available. (*Source:* U.S. Climate Prediction Center).

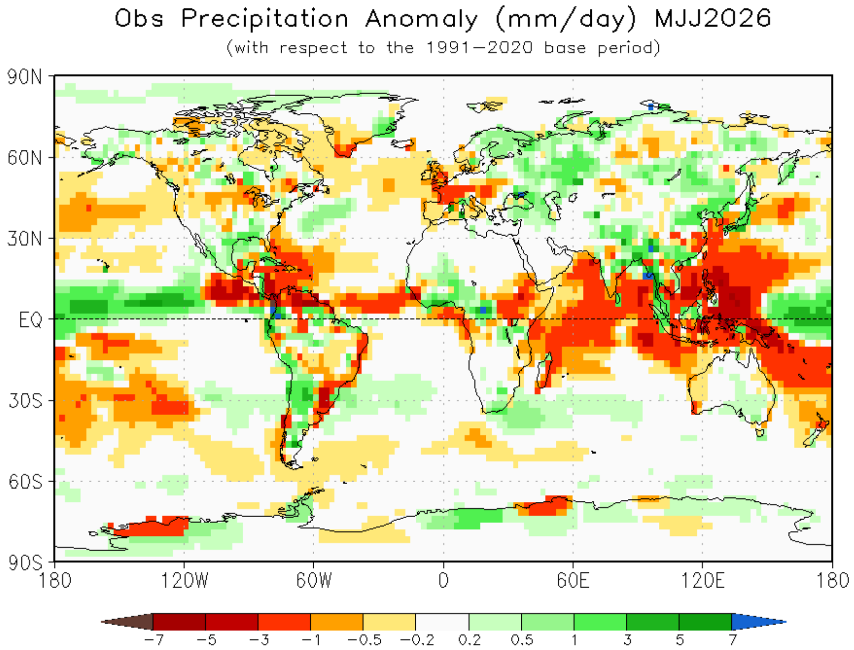

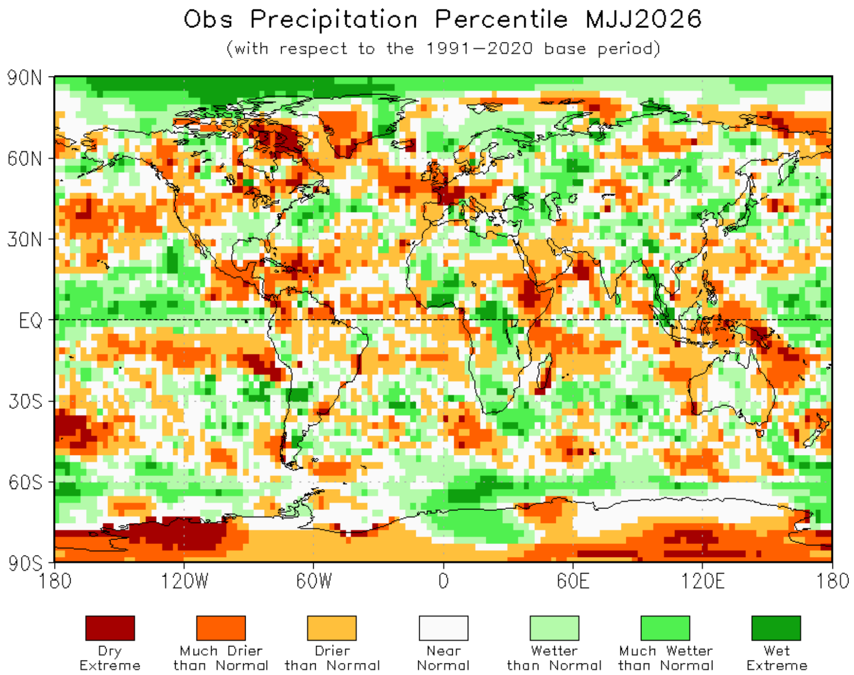

Figure 3. Observed rainfall anomalies (mm/day) for May-July 2026, relative to 1991–2020 base period (top). The *Drier than Normal, Near Normal and Wetter than Normal* shadings on the percentile map (bottom) indicate that seasonal mean anomalies were in the bottom, middle, and upper tercile of the 1991–2020 distribution, respectively. Regions with anomalies in the lowest and highest decile (or 10%) of the distribution are marked as *Much Drier than Normal* and *Much Wetter than Normal*, respectively. The *Dry Extreme* and *Wet Extreme* shadings indicate that the anomalies exceeded the driest and wettest values of the 1991–2020 period for the season. (*Source:* U.S. Climate Prediction Center)

2. Predicted evolution of the state of the climate over the next three months: September-November 2026

2.1 Large-scale SST-based indices

For the September–November 2026 (SON 2026) season, multi-model ensemble (MME) forecasts indicate a further development toward stronger El Niño conditions. The seasonal average Niño 3.4 SST ensemble mean anomaly is forecast to reach approximately 3.6°C during SON 2026, with the intensification trajectory peaking in November-December (Figure 7, left). The spread among individual forecast systems generally remains narrow, reflecting high forecast confidence.

In the Indian Ocean, a positive IOD phase is also expected to develop, reaching an SON 2026 seasonal mean value of 0.9°C. Meanwhile, the equatorial Atlantic basin is forecast to remain generally warm, with SSTs in both the North and South Tropical Atlantic staying above normal.

Month	Nino 1+2	Nino 3	Nino 4	Nino3.4	IOD	NTA	STA
September 2026	3.9±1.0	3.6±0.6	1.8±0.4	3.2±0.2	0.8±0.2	0.5±0.3	0.6±0.2
October 2026	3.9±1.1	3.9±0.8	2.0±0.5	3.6±0.4	1.0±0.3	0.6±0.3	0.7±0.3
November 2026	4.0±1.2	4.2±0.9	2.1±0.5	3.9±0.5	0.8±0.3	0.6±0.3	0.8±0.3
September-November 2026	3.9±1.1	3.9±0.7	1.9±0.4	3.6±0.4	0.9±0.3	0.6±0.3	0.6±0.3

Table 2: Multi-model forecasts for oceanic indices (°C), with standard deviation (ºC). (*Source:* The WMO Lead Centre for Seasonal Prediction Multi-Model Ensemble)

2.2 Predicted temperature

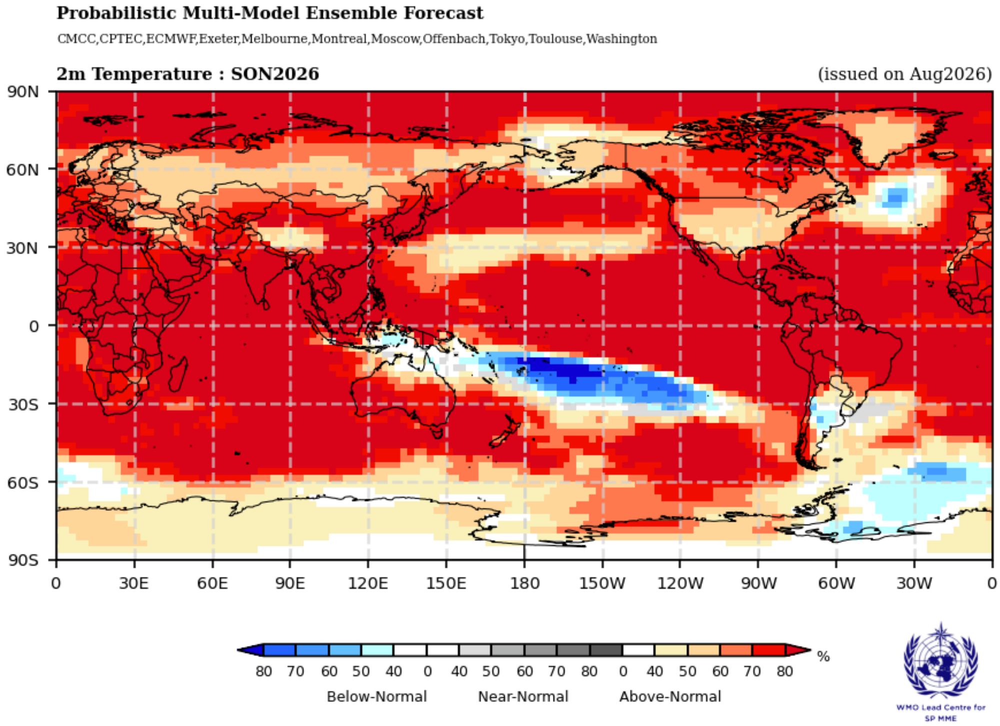

Figure 4. Probabilistic forecasts of surface air temperature for September-November 2026. The tercile category with the highest forecast probability is indicated by shaded areas. The most likely category for below-normal, above-normal, and near-normal is depicted in blue, red, and grey shadings, respectively. White areas indicate equal chances for all categories in both cases. The baseline period is 1993–2009. (*Source:* The WMO Lead Centre for Seasonal Prediction Multi-Model Ensemble)

For the SON 2026 season, multi-model ensemble forecasts project a nearly universal global dominance for enhancement in probabilities for above-normal temperatures over landmasses. This warming trend is especially pronounced north of 60°S, where a large increase in probabilities for above-normal temperature is reinforced by high model consistency (Figure 4).

In the Northern Hemisphere, a large increase in probabilities for above-normal temperatures covers Africa, southern Europe, the Arabian Peninsula, the Indian Subcontinent, eastern Asia, western coastal parts of North America below 60°N, northeastern regions of North America, Central America, the Caribbean, and the Arctic Circle above 60°N. Model consistency across these regions is moderate to strong. Conversely, a weaker enhancement in probabilities of above-normal temperatures is indicated over parts of northern Asia, as well as northwestern and central regions of North America.

In the Southern Hemisphere, a strong enhancement in probabilities for above-normal temperatures is centred over southern Africa, South America (between the equator and 30°S), most of Australia, and across New Zealand, supported by strong model consistency.

In the tropics, a large increase in probabilities for above-normal temperatures covers equatorial Africa, South America, and western parts of the Maritime Continent. Over the ocean basins, forecasts reflect the footprint of a strong El Niño event. Extreme probabilities (exceeding 80%) for above-normal SSTs dominate the equatorial Pacific east of the Date Line, where the core of the warm region displays maximum model consistency.

A widespread tendency for an increase in probabilities for above-normal temperatures also covers the Indian Ocean and the tropical Atlantic. In contrast, a region of enhancement for below- to near-normal temperature probabilities is predicted across the subpolar North Atlantic. Additionally, a distinct zone of enhanced probabilities for below-normal temperatures is centred in the South Pacific subtropical region (between 10°S and 30°S) situated directly south of the core El Niño region, supported by strong model consistency.

RA I (Africa): Over the entireregion, the multi-model ensemble forecasts project an extensive, robust enhancement in probabilities (in excess of 70%) for above-normal temperatures, supported by strong model consistency.

RA II (Asia): For this region, there is a strong enhancement in probabilities for above-normal temperature, particularly south of 50°N, covering the Arabian Peninsula, the Indian Subcontinent, Southeast Asia, and Eastern Asia. This enhancement in probabilities is supported by strong model consistency. North of 50°N, there is a weaker enhancement in probabilities for above-normal temperature, with probability signals gaining strength again north of 60°N.

RA III (South America): The largest increase in probabilities for above-normal temperature is focused north of 30°S, supported by strong model consistency. South of 30°S, there is an abrupt transition to a much weaker enhancement in above-normal temperature probabilities, which gives way to a weak enhancement in below-normal temperature probabilities in the interior part of the continent. Model agreement in this southern transition zone is generally weak. Conversely, the western coastal regions south of 30°S are predicted to feature a stronger enhancement in probabilities for above-normal temperature.

RA IV (North America, Central America, and the Caribbean): Multi-model ensemble forecasts project widespread, robust enhancements in probabilities for above-normal temperatures across southern and eastern domains. Strong enhancements in probabilities (exceeding 70–80%) supported by strong model consistency cover Central America, the Caribbean, and coastal western and northeastern parts of North America. Conversely, northwestern and central regions of North America exhibit a weaker enhancement in probabilities for above-normal temperature, with model agreement remaining low to moderate across the interior continent.

RA V (Southwest Pacific): Strong enhancements in probabilities for above-normal temperature dominate the western parts of the Maritime Continent, most of Australia, and New Zealand, supported by strong model consistency. In Australia, the strongest probability signals cover central, southern, and eastern regions. Over the oceanic domain, the central and eastern equatorial Pacific east of the Date Line features extreme probabilities (exceeding 80%) for above-normal temperatures, backed by maximum model consistency associated with the core El Niño signal. In contrast, a prominent zone of enhanced probabilities for below-normal temperatures is centered in the South Pacific subtropical region (between 10°S and 30°S, and east of the Date Line), situated directly south of the warm equatorial core, with strong model agreement.

RA VI (Europe): Multi-model ensemble forecasts project a marked latitudinal gradient in probabilities. A strong enhancement in probabilities for above-normal temperature covers southern and central parts of Europe, supported by moderate to strong model consistency. Farther north, across northern Europe and Scandinavia, there is a weaker enhancement in probabilities for above-normal temperature, accompanied by lower model consistency.

2.2 Predicted rainfall

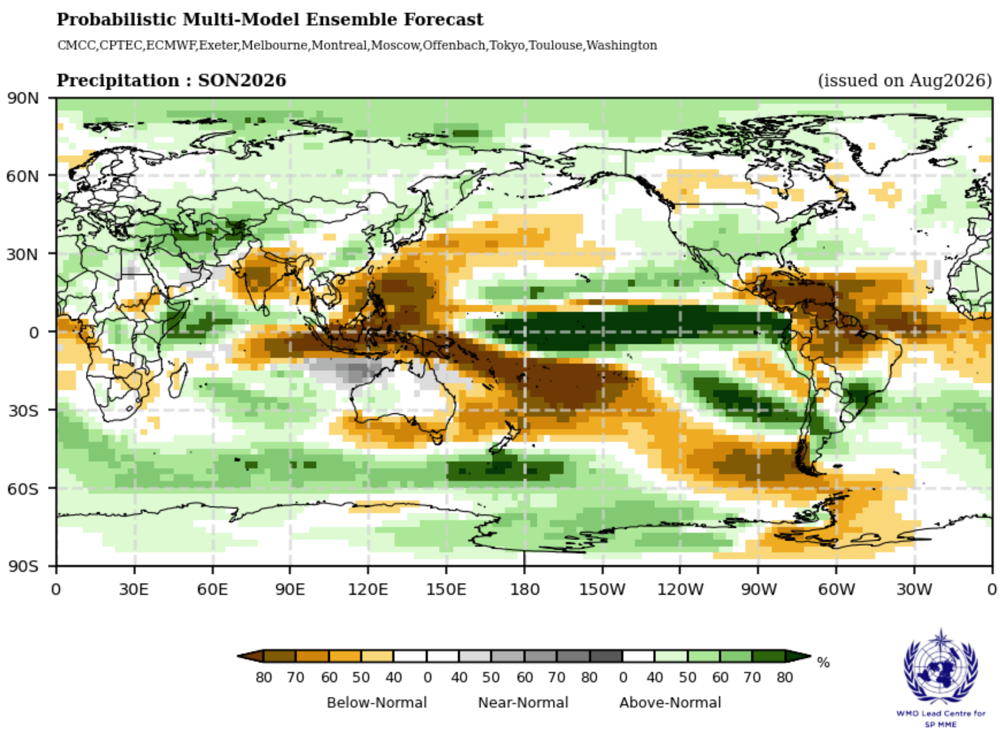

Figure 5. Probabilistic forecasts of rainfall for the season for September-November 2026. The tercile category with the highest forecast probability is indicated by shaded areas. The most likely category for below-normal, above-normal, and near-normal is depicted in orange, green and grey shadings, respectively. White areas indicate equal chances for all categories in both cases. The baseline period is 1993–2009. (*Source:* The WMO Lead Centre for Seasonal Prediction Multi-Model Ensemble)

For the SON 2026 season, MME forecasts display well-structured, large tilts in rainfall probabilities, exhibiting a classic, strong atmospheric response to Pacific El Niño (Figure 5). The most dominant feature of the SON 2026 outlook is a strong enhancement in the probability of above-normal rainfall stretching across the central and eastern equatorial Pacific east of the Date Line, backed by strong model consistency. The core for this rainfall signal is flanked by an extensive region of below-normal rainfall probabilities to the east and the west. This broad dry signal encompasses widespread marine zones, manifesting as strong enhancements in the probability for below-normal rainfall over both the tropical Indian Ocean and the equatorial Atlantic Ocean, as well as a horseshoe pattern extending into the Northern and Southern Hemispheres starting at around 120°E. The southern lobe of enhancement in below-normal probability stretches across the South Pacific to the southern tip of South America.

The Indian Subcontinent features an enhancement in the probability for below-normal rainfall, exhibiting high model consistency across the region. To its northwest, there is an enhancement in probabilities for above-normal rainfall extending into parts of Central Asia and northern regions of the Arabian Peninsula. Across equatorial Africa, the Greater Horn of Africa shows an enhanced probability for above-normal rainfall, with an enhancement in probability for below-normal rainfall to its west. Flanking this equatorial belt, a weak enhancement in the probability for above-normal rainfall is indicated over northern Africa.

Over North America, there is an enhancement in the probability for below-normal rainfall covering the southern parts of Central America and the Caribbean, supported by high model consistency. To its north, there is an enhancement in the probability of above-normal rainfall over parts of North America south of 45°N. In South America, a robust enhancement in probability for below-normal rainfall is centered over the northwest, continuing steadily along the northern coastal areas to the east. Farther south, a branch of enhanced probability for above-normal rainfall extends across southeastern South America, giving way to an enhanced probability for below-normal rainfall over the southern tip of the continent.

Across Europe, the forecasts reveal a notable latitudinal split. An enhancement in the probability of above-normal rainfall covers the southern parts of Europe, whereas the predicted signal is weak across northern Europe. The consistency is low to moderate.

Over Australia, the predicted signal is weak.

RA I (Africa): There is a marked east-west contrast in precipitation probabilities across the equatorial zone. The Greater Horn of Africa exhibits an enhanced probability for above-normal rainfall, whereas equatorial West Africa, extending westward from Central Africa, shows an enhanced probability for below-normal rainfall. Flanking this equatorial belt to the north, a weak enhancement in the probability for above-normal rainfall is indicated over northern Africa. Over southern Africa, the rainfall signal is generally weak to neutral, with localized enhancements in below-normal rainfall probabilities along eastern coastal areas.

RA II (Asia): Multi-model ensemble forecasts indicate significant spatial contrasts in precipitation probabilities. A robust enhancement in the probability for below-normal rainfall dominates the Indian Subcontinent, supported by high model consistency across the region. Conversely, to itsnorthwest, an enhancement in probabilities for above-normal rainfall extends across northern parts of the Arabian Peninsula into Central Asia. Over northern parts of Asia, a weak enhancement in above-normal rainfall probability is indicated. Over East Asia and Southeast Asia, the rainfall signal is more nuanced: an enhancement in below-normal rainfall probabilities covers southern and insular Southeast Asia (extending into the western Maritime Continent), whereas parts of northeastern Asia exhibit localized enhancements in above-normal rainfall probabilities.

RA III (South America): For this region, there is a marked regional contrast driven by the equatorial Pacific El Niño footprint. A robust enhancement in the probability for below-normal rainfall is centered over the northwestern part of the continent, extending steadily eastward along the northern coastal regions. Farther south, a distinct branch of enhanced probability for above-normal rainfall spans southeastern South America. Over the southern tip of the continent , this wet signal gives way to an enhancement in the probability for below-normal rainfall, supported by the southern lobe of the Pacific dry anomaly belt.

RA IV (North America, Central America, and the Caribbean): An enhancement in the probability for below-normal rainfall covers southern parts of Central America and the Caribbean, supported by high model consistency. To the north, an enhancement in the probability for above-normal rainfall extends across parts of North America south of 45°N. Over northern regions of North America and southern Greenland, the precipitation signal is generally weak, except for localized enhancements in below-normal rainfall probabilities over far northeastern North America.

RA V (Southwest Pacific): Across this region there are large-scale shifts in rainfall probabilities, reflecting a classic El Niño signal. A broad, robust enhancement in the probability for below-normal rainfall encompasses the Maritime Continent and extends southeastward across the South Pacific as part of a prominent horseshoe pattern. In contrast, extreme probabilities for above-normal rainfall dominate the central and eastern equatorial Pacific east of the Date Line, backed by high model consistency. Across Australia, the predicted rainfall signal is generally weak and spatially incoherent, while New Zealand shows a weak inclination in probability toward below-normal rainfall in the north and toward above-normal rainfall at the southern tip.

RA VI (Europe): Multi-model ensemble forecasts reveal a notable latitudinal split in precipitation probabilities. An enhancement in the probability for above-normal rainfall covers southern parts of Europe, supported by low-to-moderate model consistency. In contrast, the predicted rainfall signal is generally weak and neutral across northern Europe, with no strong, coherent model consensus.

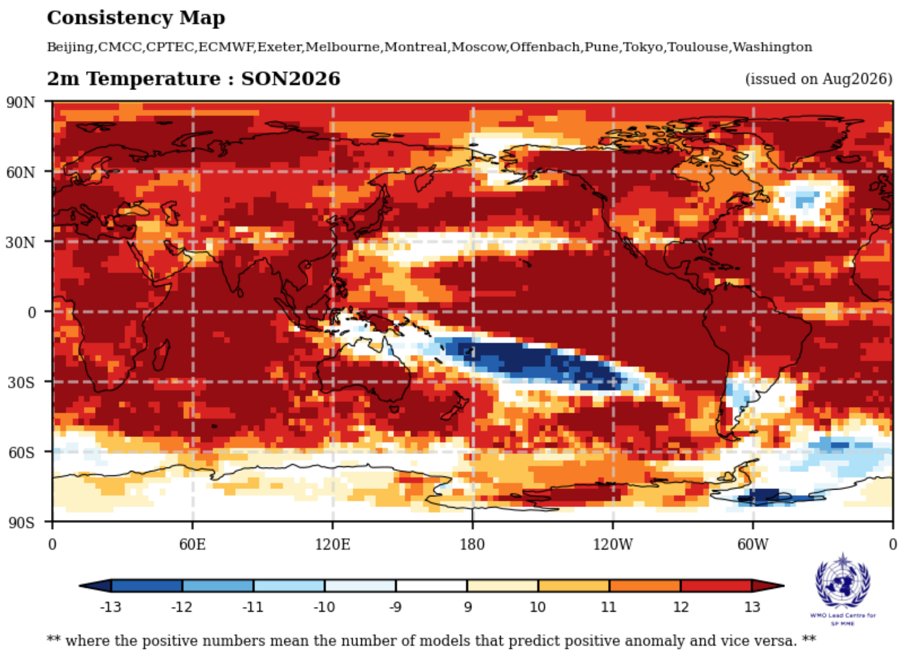

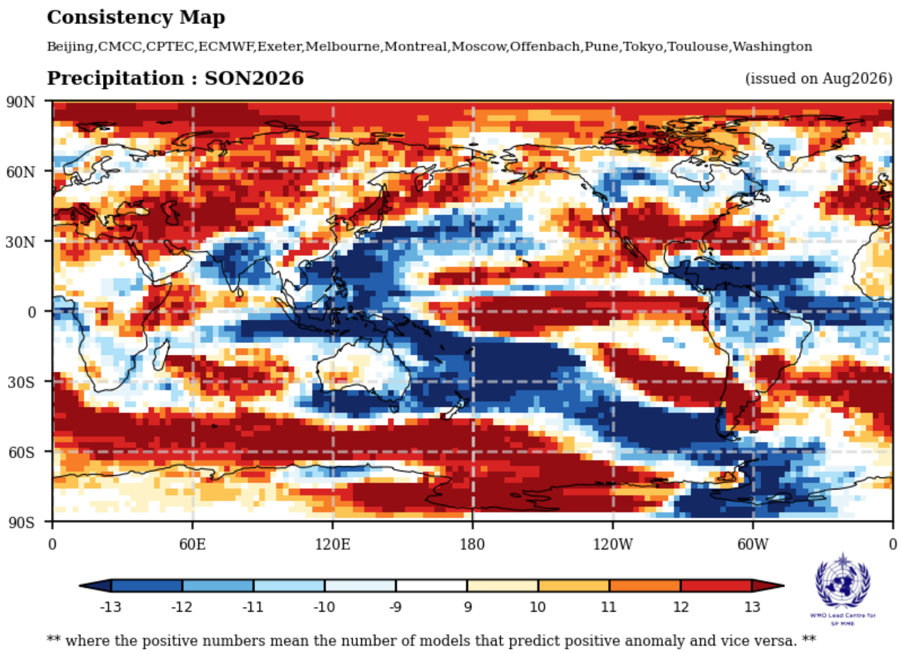

Figure 6. Consistency maps for sign of ensemble mean anomalies for the seasonal mean of September-November 2026 for surface air temperature (top) and rainfall (bottom) from different model forecasts. The consistency map is constructed using the following procedure: At each grid point the number of models with positive or negative anomaly is counted and the number that is larger in plotted on the map. For example, if the number of models with positive (negative) anomaly is larger than the count is plotted on the map using the red (blue) scale. Darker (lighter) colours imply that there is a higher (lower) consistency in the sign of anomalies between models. (*Source:* The WMO Lead Centre for Seasonal Prediction Multi-Model Ensemble)

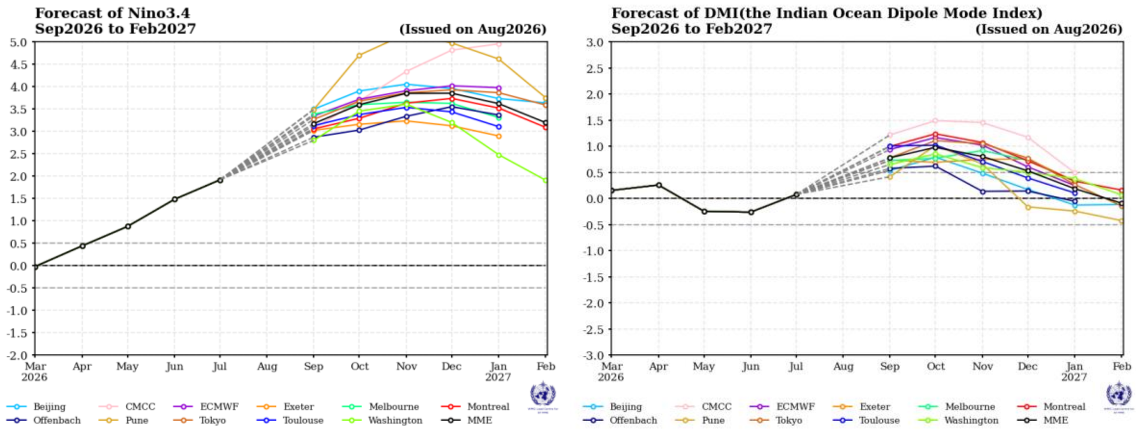

Figure 7. Evolution of Niño 3.4 (left) and Indian Ocean Dipole (IOD) (right) anomalies from August 2026 initial conditions. The solid black line represents the observed evolution, transitioning into the ensemble mean forecasts from various seasonal prediction systems (coloured lines). All anomalies are in °C relative to the 1993–2009 baseline period. (*Source:* The WMO Lead Centre for Seasonal Prediction Multi-Model Ensemble)

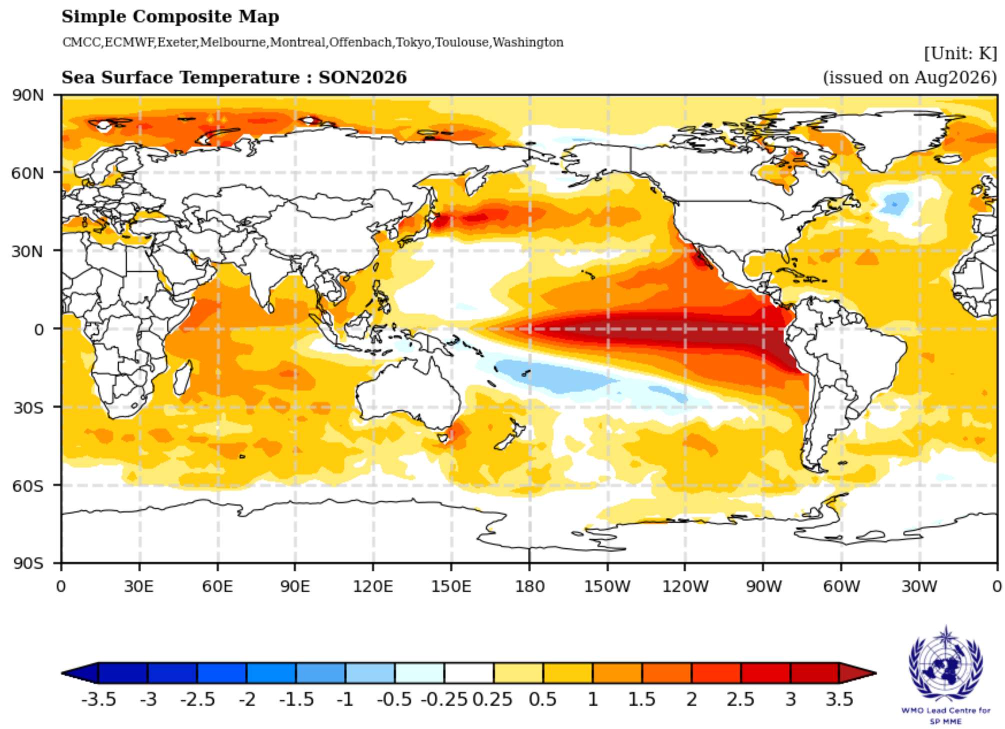

Figure 8: Multi-Model Ensemble forecast for sea surface temperature anomaly (ºC) for September-November 2026. The baseline period is 1993–2009. (*Source:* The WMO Lead Centre for Seasonal Prediction Multi-Model Ensemble)

3. Latest updates for monitoring and prediction information

Each month, the latest updates for the real-time monitoring and seasonal mean predictions included in GSCU can be found at:

Monitoring:

https://ftp.cpc.ncep.noaa.gov/mingyue/GSCUWMO/

Predictions:

www.wmolc.org/board/downloadExt?fn=WMOLC_T2M.png

http://www.wmolc.org/board/downloadExt?fn=WMOLC_PREC.png

4. How to use the Global Seasonal Climate Update

The GSCU is intended as guidance for RCCs, Regional Climate Outlook Forums (RCOFs) and National Meteorological and Hydrological Services (NMHSs). It does not constitute an official forecast for any region or nation. Seasonal outlooks for any region or nation should be obtained from the relevant RCCs (see below for contact details) or NMHS.

Figure 4 shows the spatial pattern of seasonal mean surface air temperature forecast probabilities. Probabilities are calculated for the temperature for the season being in the highest third (above-normal or warm), middle third (normal) or lowest third (below-normal or cold) ranges of the baseline record (1993-2009) at each location. Colour code is indicated only for the category that has the highest forecast probability. For example, for regions highlighted in red, the most likely forecast category for seasonal mean surface air temperature to occur is warmer than normal. Similarly, the blue colour highlights regions where the seasonal mean surface air temperature forecast indicates the colder than normal category as most likely, while grey colour highlights regions where the seasonal mean temperature forecast indicates the near normal category as most likely. Deeper shades of respective colours highlight increasing probability for the seasonal mean temperature to be in the indicated category. White areas indicate equal chances for all categories.

A particular colour does not assure that the seasonal mean temperature is "certain" to be observed in the most likely forecast category that is shown, but rather its probability of being in that category. Consequently, the observed seasonal mean temperatures have a non-zero probability to be observed in a category different from the category indicated on the map as most likely. Users need to take the probabilistic nature of seasonal forecasts into account when making decisions.

It should also be noted that the absolute values for the surface air temperature corresponding to the definitions of the above normal (warm), normal or below normal (cold) categories depend on the climatology (historical information) at the location, and therefore, is location dependent.

The interpretation of the probabilities for the rainfall forecast (Figure 5) is the same as that for the seasonal mean surface air temperature except that green and brown colours indicate whether the forecasted seasonal mean rainfall is most likely to be in the wet or dry category. As for surface temperature, grey colour highlights regions where the seasonal mean rainfall forecast indicates the near normal category as the most likely.

The skill of seasonal forecasts is substantially lower than that of weather timescales and skill varies considerably with region and season.

For further details on seasonal predictions see: Guidance on Operational Practices for Objective Seasonal Forecasting

For reference, the six WMO Regional Associations domains are depicted in the figure below.

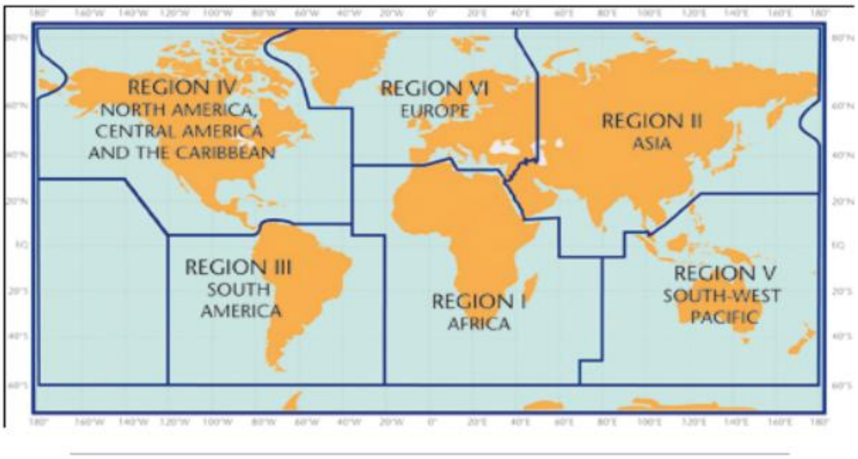

5. Designated and developing WMO Regional Climate Centres and Regional Climate Centre Networks

- https://public.wmo.int/en/our-mandate/climate/regional-climate-centres

6. Resources

Sources for the graphics used in the GSCU:

- The WMO Lead Centre for Seasonal Prediction Multi-Model Ensemble (LC-SPMME): http://www.wmolc.org
- WMO portal to the Global Producing Centres for Seasonal Prediction (GPCs-SP): https://public.wmo.int/en/programmes/global-data-processing-and-forecasting-system/global-producing-centres-of-long-range-forecasts
- WMO portal for Regional Climate Outlook Forums https://public.wmo.int/en/our-mandate/climate/regional-climate-outlook-products
- NOAA Climate Prediction Centre (CPC): http://www.cpc.ncep.noaa.gov ; https://www.cpc.ncep.noaa.gov/products/people/mchen/AttributionAnalysis/

7. Acknowledgements

This Global Seasonal Climate Update was jointly developed by the WMO Infrastructure (INFCOM) and Services (SERCOM) Commissions with contributions from:

- WMO Lead Centre for Seasonal Prediction Multi-Model Ensemble (LC-SPMME), Korea Meteorological Administration, NOAA National Centers for Environmental Prediction

- WMO Global Producing Centres for Seasonal Prediction (GPCs-SP): GPC-Beijing (China Meteorological Administration), GPC-CPTEC (Center for Weather Forecast and Climate Studies, Brazil), GPC-ECMWF (European Center for Medium-Range Forecast), GPC-Exeter (UK Met Office),GPC- Melbourne (Bureau of Meteorology), GPC-Montreal (Meteorological Services of Canada), GPC-Moscow (Hydro meteorological Center of Russia), GPC-Offenbach Deutscher Wetterdienst), GPC-Pretoria (South African Weather Services), GPC-Seoul (Korea Meteorological Administration), GPC-Tokyo (Japan Meteorological Agency), GPC-Toulouse (Météo-France), GPC-Washington (National Centers for Environmental Prediction), GPC-CMCC (Centro Euro-Mediterraneo sui Cambiamenti Climatici), GPC-Pune (India Meteorological Department).